September 2010

Editors: A. Cooper-Sarkar, S. Glazov, K. Lipka, R. Plačakytė, V. Radescu
H1-prelim-10-143, ZEUS-prel-10-019

The Rôle of the Charm Mass Parameter in the QCD Analysis of the Combined HERA Data and Implications for the LHC

H1 and ZEUS Collaborations

Abstract

A next-to-leading order QCD analysis is performed to the preliminary combination of the H1 and ZEUS $F_2^{c\bar{c}}$ measurements together with the published HERA inclusive neutral and charged current cross sections. Different models in variable flavour number scheme were used for the heavy flavour treatment. The fits are used to estimate the optimal value of the charm quark mass parameter $m_c^{\rm model}$ within a given heavy flavour scheme. Depending on the scheme, the optimal values of $m_c^{\rm model}$ range between 1.26 GeV and 1.68 GeV, and are determined with a precision of 0.04 GeV including statistical, model and parameterisation uncertainties. The parton distribution functions determined using the above heavy quark schemes at their optimal values of $m_c^{\rm model}$ are further used to predict the $W^\pm$ and Z production cross sections at the LHC. Good agreement between these predictions for the $W^\pm$ and Z cross sections is observed which allows to reduce the uncertainty due to the heavy flavour treatment, to below 1.0%.

1 Introduction

The combined H1 and ZEUS inclusive $e^{\pm}p$ Deep Inelastic Scattering (DIS) cross sections from HERA I and the next-to-leading order (NLO) Quantum Chromodynamic (QCD) analysis have been recently published [1]. In this set, the combination of the Neutral and Charged Current (NC and CC) data allows for the following PDF separation: gluon $xg(x)$; valence $xu_v(x)$, $xd_v(x)$ as well as $u-$ and d type sea $x\bar{U}(x) = x\bar{u}(x)$, $x\bar{D}(x) = x\bar{d}(x) + x\bar{s}(x)$ densities at the evolution starting scale below the charm quark mass. The heavy quark densities are calculated following various implementations of the variable flavour number schemes (VFNS).

At NLO, VFNS have a significant ambiguity in describing the onset of the heavy quark densities at the scales Q comparable with the heavy quark pole masses for the charm and bottom quarks, m_c and m_b, respectively. Different approaches for the interpolation function and counting of orders in α_S lead to a number of VFNSs, four of which, S-ACOT-χ [2], ACOT-full [3], RT [4,5], RT-optimised [5], are considered in this note. The zero mass variable flavour number scheme (ZMVFNS) was also considered in this analysis. In all schemes, the onset of the heavy quarks is controlled by the parameter $m_{b,c}^{\rm model}$.

In DIS heavy quarks are produced dominantly via boson-gluon fusion. At HERA, the charm contribution to the total DIS cross section is significant and reaches about 30% at large values of Q^2. The beauty contribution is an order of magnitude smaller. In the HERAPDF1.0 analysis, the uncertainty due to the heavy flavour treatment is estimated by varying $m_{b,c}^{\rm model}$ within the ranges of $1.35 < m_c^{\rm model} < 1.65$ and $4.3 < m_b^{\rm model} < 5.0$ GeV. The variation of $m_b^{\rm model}$ shows a small influence on the resulting PDFs (apart from $x\bar{b}(x)$ itself). In contrary, the variation of $m_c^{\rm model}$ results in significant change of the gluon distribution which leads consequently to the change of the sea quark densities. In particular, the suppression of $x\bar{c}(x)$ in the sea distribution is compensated by the increase of $x\bar{u}(x)$.

In a recent preliminary combination of the H1 and ZEUS $F_2^{c\bar{c}}$ measurements [6] a precision of $5 - 10\%$ has been achieved. The kinematic range of the data, $2 \leq Q^2 \leq 1000$ GeV^2, include the region sensitive to the heavy quark thresholds. In this note, these charm data are used together with different implementations of VFNSs. The accuracy of the data should allow to reduce the ambiguity in the separation of $x\bar{U}(x)$ into $x\bar{u}(x)$ and $x\bar{c}(x)$ contributions. A QCD analysis is therefore performed including the charm data together with inclusive DIS cross sections in order to extract PDFs and to determine the optimal $m_c^{\rm model}$ value for each of the VFNS investigated. With the resulting PDFs predictions for the $W^{\pm}$ and Z cross sections at the LHC are calculated.

The note is organised as follows. In section 2, the data sets and the QCD fit are introduced. In Section 3 the determination of $m_c^{\rm model}$ for each VFNS and extraction of the corresponding PDF sets are described. The predictions for $W^{\pm}$ and Z boson production cross sections are presented in section 4.

2 Data and QCD Fit Settings

The preliminary combined charm data are used together with the published combined measurement of inclusive DIS cross sections at HERA [1] as input to a QCD fit based on the DGLAP

NLO evolution scheme. For this purpose, the program QCDNUM [7] is used. The minimum invariant mass W of the hadronic system is 15 GeV and the value of the Bjorken scaling variable is restricted to $x \leq 0.65$. Therefore target mass corrections and higher twist contributions are expected to be small. Furthermore, the analysis is restricted to $Q^2_{min} = 3.5$ GeV^2 to assure the applicability of pQCD. The consistency of the input data set and the control on the systematic uncertainties enable the calculation of the experimental uncertainties on the PDFs using the χ^2 tolerance of $\Delta\chi^2 = 1$.

In the fit procedure, the following independent PDFs are chosen: $xu_v(x)$, $xd_v(x)$, $xg(x)$ and $x\bar{U}(x)$, $x\bar{D}(x)$, where $x\bar{U}(x) = x\bar{u}(x)$, and $x\bar{D}(x) = x\bar{d}(x) + x\bar{s}(x)$ at the starting scale Q_0 below the charm mass. The default PDFs at the starting scale $Q_0^2 = 1.9$ GeV^2, is given by

$$xf(x) = Ax^B(1-x)^C(1+Ex^2). \tag{1}$$

The parameterisation and the constraints on the parameters are the same as for the central PDF of HERAPDF1.0 [1]. The PDFs are evolved using DGLAP evolution equations [8–12] at NLO [13,14] in the $\overline{\text{MS}}$ scheme with the renormalisation and factorisation scales set to Q^2 and the strong coupling set to $\alpha_s(M_Z) = 0.1176$ [15].

The QCD predictions for the structure functions are obtained by convolution of the PDFs with the NLO coefficient functions calculated using different implementations of the general mass variable favour number scheme: ACOT full [3] as used for the CTEQHQ releases of PDFs, S-ACOT-χ [2] as used for the latest CTEQ releases of PDFs, RT scheme [4,5] as used for the MRST and MSTW releases of PDFs, as well as an optimised RT scheme providing a smoother behaviour across thresholds [5]. The ZMVFNS as implemented by the NNPDF group [16] is also used.

Since the study involves variations of the charm mass parameter down to $m_c^{\text{model}} = 1.2$ GeV and the evolution starting scale must be chosen below $(m_c^{\text{model}})^2$, fits are performed with a starting scale of $Q_0^2 = 1.4$ GeV^2. As it was shown in [1], the gluon density at this starting scale could not be well described by a parameterisation form of equation 1 and it is therefore modified to

$$xg(x) = A_g x^{B_g}(1-x)^{C_g} - A'_g x^{B'_g}(1-x)^{25}\,, \tag{2}$$

which allows for more flexible shapes of the gluon PDF and the low starting scale. The choice of the exponent in the $(1-x)$-term is motivated by the approach of the MSTW group. Other variants of the PDF parameterisations which proved to have an effect on HERAPDF1.0 have been considered and included in the evaluation of the systematic uncertainties for m_c^{model}.

3 Determination of Optimal m_c^{model}

In each heavy flavour scheme PDF fits were performed by varying m_c^{model} from 1.2 GeV to 1.8 GeV. For each fit the χ^2 value is calculated and the optimal value $m_c^{\text{model}}(\text{opt})$ is subsequently determined from a parabolic fit to the χ^2 data of a form

$$\chi^2(m_c^{\text{model}}) = \chi^2_{\min} + \left(\frac{m_c^{\text{model}} - m_c^{\text{model}}(\text{opt})}{\Delta_{m_c^{\text{model}}(\text{opt})}}\right)^2, \tag{3}$$

where $\chi^2_{\min}$ is the χ^2 value at the minimum and $\Delta_{m_c^{\text{model}}(\text{opt})}$ is the experimental uncertainty on $m_c^{\text{model}}(\text{opt})$.

The scanning procedure is illustrated in figures 1-2 for the standard RT scheme. First the HERAPDF1.0 datasets, i.e. the H1 and ZEUS combined inclusive NC and CC cross sections from HERA I [1] are used (figure 1), not including the charm $F_2^{c\bar{c}}$ data. In this case, χ^2 varies only little with m_c^{model} in the range 1.2 GeV to 1.8 GeV. When the charm data are included, χ^2 is much more sensitive to m_c^{model} (figure 2). Fits using the standard and flexible gluon parameterisation show very similar behaviour. Figures 3-6 illustrate the χ^2 scans for the optimised RT, ACOT full, S-ACOT-χ and ZMVFN schemes. Figure 7 summarises the study by showing the m_c^{model} scanning results for all schemes together. It is interesting to observe that $\chi^2_{\min}$ values are comparable for all schemes despite different values of $m_c^{\text{model}}(\text{opt})$. Values of $\chi^2_{\min}$ are almost identical for standard RT, optimised RT and ACOT full schemes, and are worse by ~ 20 units for the S-ACOT χ scheme and by ~ 50 units for the ZMVFN scheme.

The experimental uncertainty on $m_c^{\text{model}}(\text{opt})$ includes the model, parameterisation and α_S uncertainty, following the prescription of [1]. In this procedure, for each VFN scheme the fitting assumptions are varied one by one and m_c^{model} scans are repeated around the $m_c^{\text{model}}(\text{opt})$ value obtained from the central fits. Typically, uncertainties in $m_c^{\text{model}}(\text{opt})$ are increased by factor two compared to experimental errors only with exception of the ZMVFN scheme for which the uncertainty is increased by a factor of ~ 3.

In Figure 8 the $F_2^{c\bar{c}}$ data are compared with fits using different VFN schemes which are performed for $m_c^{\text{model}} = m_c^{\text{model}}(\text{opt})$. The comparison of the predictions of the individual schemes to the $F_2^{c\bar{c}}$ data are shown in Figures 9-13. These predictions describe the data well with the exception of the ZMVFN scheme at $Q^2 \leq 12$ GeV^2.The uncertainties on $m_c^{\text{model}}(\text{opt})$ are given in table 1.

4 $W^{\pm}, Z$ Production Cross Sections at the LHC

The PDFs obtained from fits to the HERA data by the m_c^{model} scanning procedure are used to calculate predictions for $W^{\pm}$ and Z production cross sections at the LHC. These predictions are calculated for $1.2 \leq m_c^{\text{model}} \leq 1.8$ GeV in 0.1 GeV steps for each of the VFN schemes using the MCFM program, version 5.7, with the same conditions as for the PDF4LHC benchmarking [17].

The $W^{\pm}$ and Z^0 cross sections as a function of m_c^{model} for the different schemes are shown in Figures 14-16 and the values for the optimal choice $m_c^{\text{model}}(\text{opt})$ are summarised in table 1.

For all VFN schemes a similar monotonic dependence of the $W^{\pm}$ and Z^0 boson production cross sections is observed. There is, however, a sizable offset between the predictions if they are considered for a fixed value of m_c^{model}: if the ZMVFN scheme is included (excluded) the difference reaches 7% (4.5%). Similarly, for each scheme the change of the prediction varies by about 7% for m_c^{model} raising from 1.2 to 1.8 GeV. However, when using the $m_c^{\text{model}}(\text{opt})$ the spread of predictions is reduced to 0.7% (2.3%) when excluding (including) the ZMVFNS calculations.

The ZMVFN scheme describes the data worst and differs significantly from the other schemes in $W^{\pm}$ and Z^0 predictions. Furthermore, the ZMVFNS does not describe the charm production in DIS at HERA even at high Q^2 [18].

scheme	$m_c^{\rm model}$(opt) GeV	χ^2/dof	χ^2/ndp $F_2^{c\bar{c}}$	σ_Z(nb)	σ_{W^+}(nb)	σ_{W^-}(nb)
RT standard	$1.58^{+0.02}_{-0.03}$	620.3/621	42.0/41	$29.27^{+0.07}_{-0.11}$	$57.82^{+0.14}_{-0.22}$	$40.22^{+0.10}_{-0.15}$
RT optimised	$1.46^{+0.02}_{-0.04}$	621.6/621	46.5/41	$29.17^{+0.07}_{-0.13}$	$57.75^{+0.14}_{-0.26}$	$40.15^{+0.10}_{-0.18}$
ACOT-full	$1.58^{+0.03}_{-0.04}$	621.2/621	59.9/41	$29.28^{+0.10}_{-0.13}$	$57.93^{+0.18}_{-0.24}$	$40.16^{+0.12}_{-0.16}$
S-ACOT-χ	$1.26^{+0.02}_{-0.04}$	639.7/621	68.5/41	$29.37^{+0.08}_{-0.15}$	$58.06^{+0.16}_{-0.30}$	$40.23^{+0.11}_{-0.21}$
ZMVFNS	$1.68^{+0.06}_{-0.07}$	667.4/621	88.1/41	$28.71^{+0.19}_{-0.20}$	$56.77^{+0.33}_{-0.34}$	$39.46^{+0.24}_{-0.25}$

Table 1: The $m_c^{\rm model}$(opt) as determined from the $m_c^{\rm model}$ scans in different heavy flavour schemes. The corresponding χ^2 per degrees of freedom dof (per number of data points ndp) values for the complete data set using inclusive and charm data (for the charm data only) are presented, as obtained using the flexible gluon parametrisation. The predictions of the Z/W cross sections at LHC are given.

5 Conclusions

Using recent preliminary $F_2^{c\bar{c}}$ data together with the published HERA I combined data, a NLO QCD analysis was performed based on different implementations of the variable flavour number scheme. For each implementation, an optimal value of the charm mass parameter $m_c^{\rm model}$ was determined. The values of optimal $m_c^{\rm model}$ show sizable spread, ranging between 1.26 GeV and 1.68 GeV. Apart from the ZMVFN scheme, all schemes were found to describe the data well, with comparable $\chi^2/\,n_{\rm dof}$, as long as $m_c^{\rm model}$ was taken at corresponding optimal values.

PDFs obtained from fits with different $m_c^{\rm model}$ were used to predict $W^\pm$ and Z production cross sections at the LHC. A sizable spread in the predictions was observed for each model when $m_c^{\rm model}$ was varied between 1.2 and 1.8 GeV, as well as when considering different schemes at a fixed value of $m_c^{\rm model}$. This spread is significantly reduced when the optimal value of $m_c^{\rm model}$ is used in each model.

This analysis has shown that the inclusion of the preliminary $F_2^{c\bar{c}}$ measurements helps to reduce the uncertainties due to the heavy flavour treatment in the PDF fit on the $W^\pm$ and Z production cross section at LHC to below 1.0% in a model independent way.

References

[1] F. Aaron *et al.* [H1 and ZEUS Collaborations], JHEP **1001**, 109 (2010), [0911.0884].

[2] W. K. Tung *et al.*, JHEP **02**, 053 (2007), [hep-ph/0611254].

[3] M. Kramer, F. I. Olness, and D. E. Soper, Phys. Rev. **D62**, 096007 (2000), [hep-ph/0003035].

[4] R. S. Thorne and R. G. Roberts, Phys. Rev. D **57**, 6871 (1998), [hep-ph/9709442].

[5] R. S. Thorne, private communication, 2008,2010.

[6] H1 and Z. Collaborations.

[7] M. Botje (2010), http://www.nikef.nl/h24/qcdnum/index.html, [1005.1481].

[8] V. N. Gribov and L. N. Lipatov, Sov. J. Nucl. Phys. **15**, 438 (1972).

[9] V. N. Gribov and L. N. Lipatov, Sov. J. Nucl. Phys. **15**, 675 (1972).

[10] L. N. Lipatov, Sov. J. Nucl. Phys. **20**, 94 (1975).

[11] Y. L. Dokshitzer, Sov. Phys. JETP **46**, 641 (1977).

[12] G. Altarelli and G. Parisi, Nucl. Phys. B **126**, 298 (1977).

[13] G. Curci, W. Furmanski, and R. Petronzio, Nucl.Phys. **B175**, 27 (1980).

[14] W. Furmanski and R. Petronzio, Phys.Lett. **B97**, 437 (1980).

[15] C. Amsler *et al.* (Particle Data Group), Phys. Lett. **B667**, 1+ (2008).

[16] R. D. B. at al. (2010), [arXiv 1002.4407].

[17] URL `https://wiki.terascale.de/index.php?title=PDF4LHC_WIKI`.

[18] e. a. F. D. Aaron, Phys. Lett. B **686**, 91 (2010), [arXiv 0911.3989].

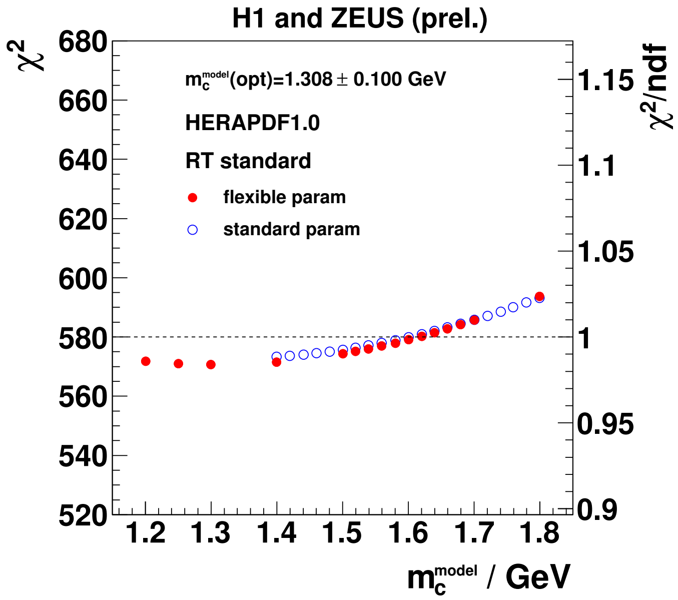

Figure 1: χ^2 *of the HERA I data fit (HERAPDF1.0) in the standard RT scheme as a function of* m_c^{model} *. Open and closed symbols represent flexible and standard parametrisation repsectively (see text for the explanation).*

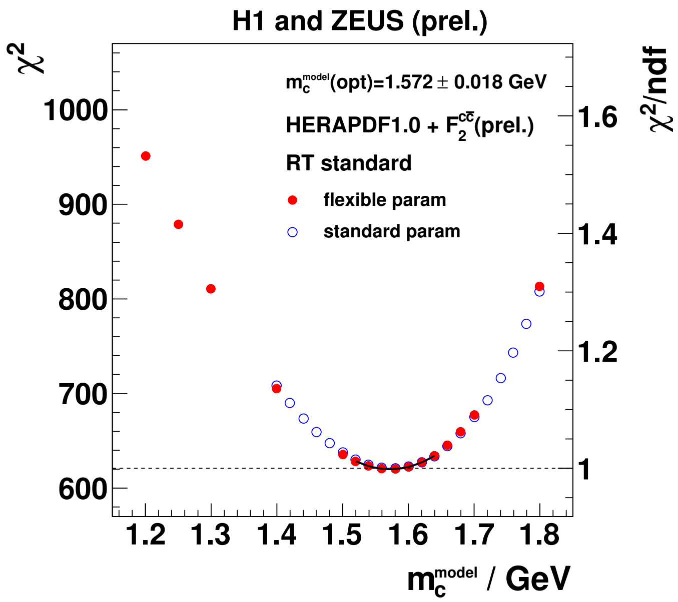

Figure 2: χ^2 *of the HERA I+*$F_2^{c\bar{c}}$ *fit in the standard RT scheme as a function of* m_c^{model} *. Open and closed symbols represent flexible and standard parametrisation repsectively (see text for the explanation).*

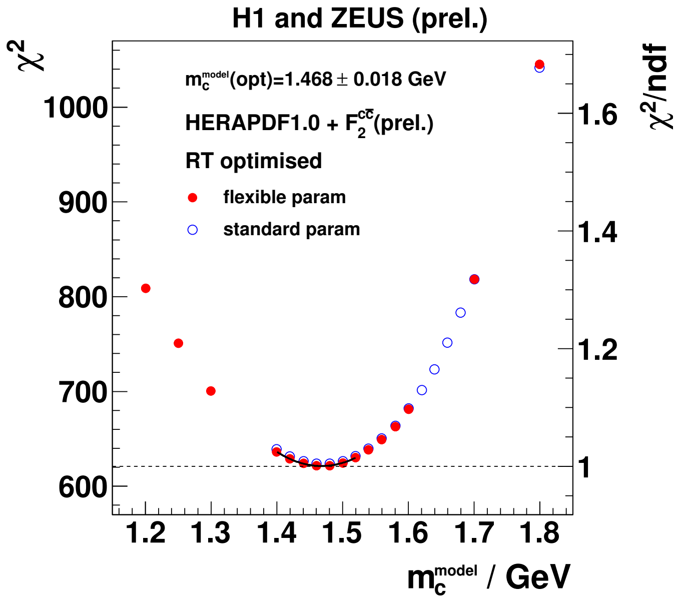

Figure 3: *χ^2 of the HERA I + $F_2^{c\bar{c}}$ fit in the optimised RT scheme as a function of m_c^{model} . Open and closed symbols represent flexible and standard parametrisation repsectively (see text for the explanation).*

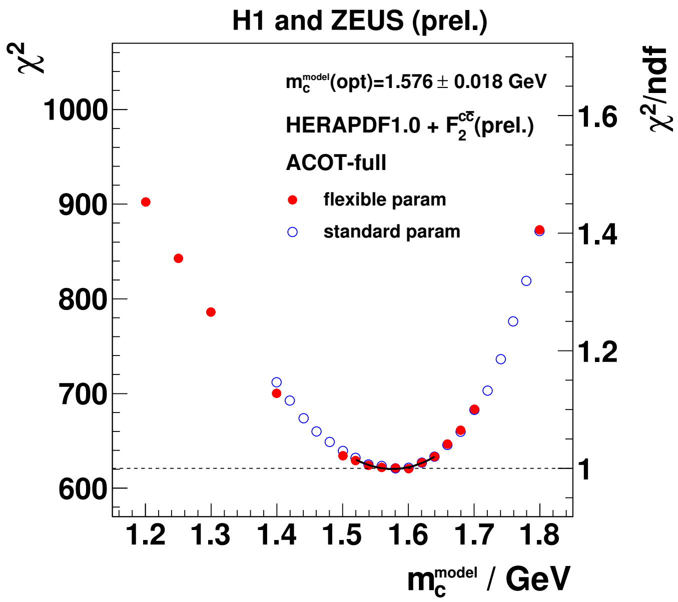

Figure 4: *χ^2 of the HERA I + $F_2^{c\bar{c}}$ fit in the ACOT-full scheme as a function of m_c^{model} . Open and closed symbols represent flexible and standard parametrisation repsectively (see text for the explanation).*

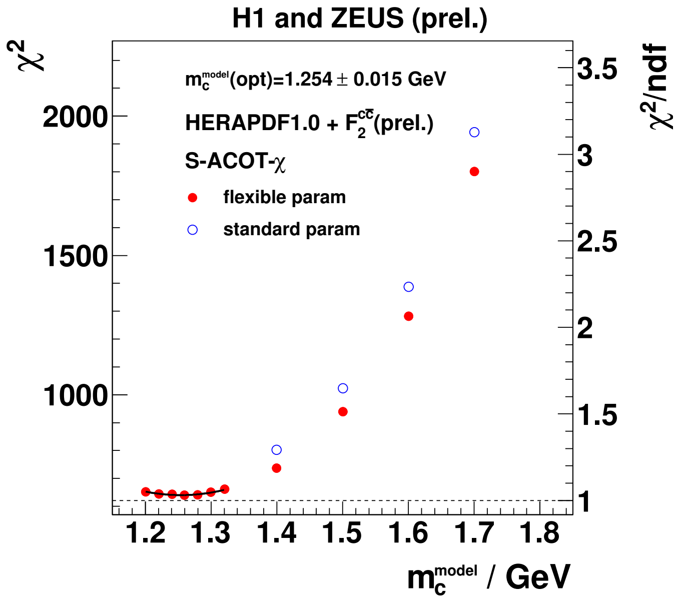

Figure 5: χ^2 *of the HERA I +* $F_2^{c\bar{c}}$ *fit in the S-ACOT-*χ *scheme as a function of* m_c^{model} *. Open and closed symbols represent flexible and standard parametrisation repsectively (see text for the explanation).*

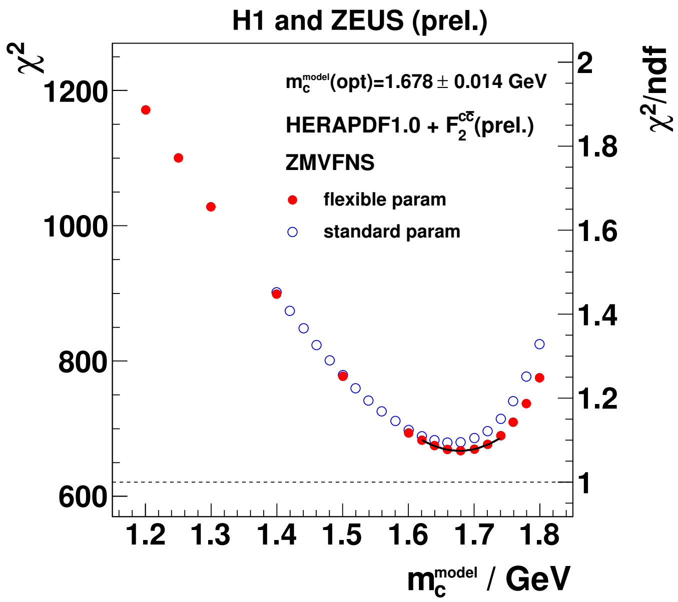

Figure 6: χ^2 *of the HERA I +* $F_2^{c\bar{c}}$ *fit in the ZMVFN scheme as a function of* m_c^{model} *. Open and closed symbols represent flexible and standard parametrisation repsectively (see text for the explanation).*

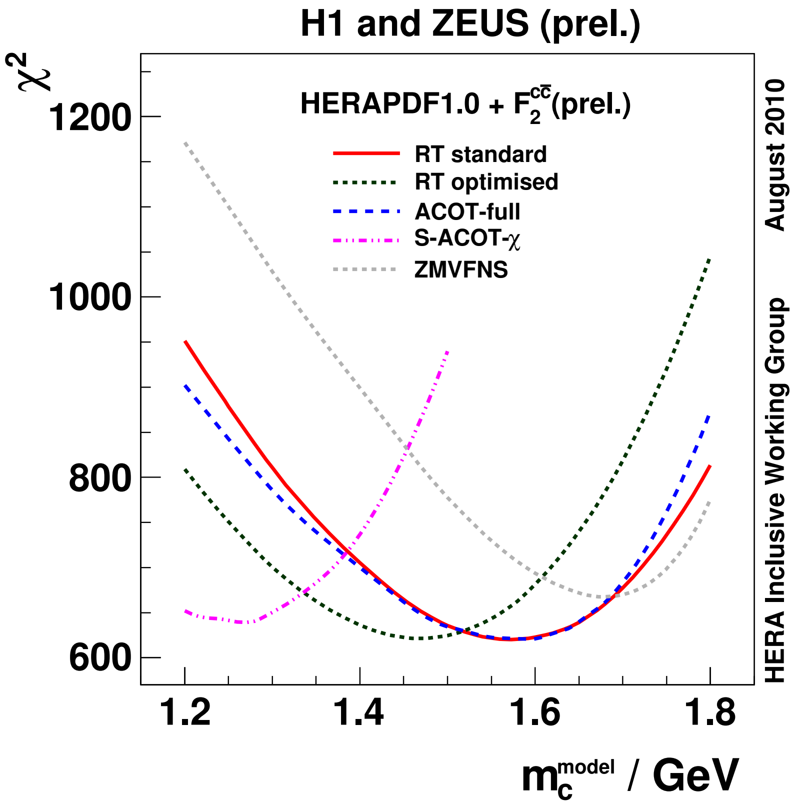

Figure 7: *Comparison of the χ^2 of HERA I + $F_2^{c\bar{c}}$ fits using different heavy flavour schemes represented as lines of different styles. The flexible parmetrisation was used for the fits shown in the figure.*

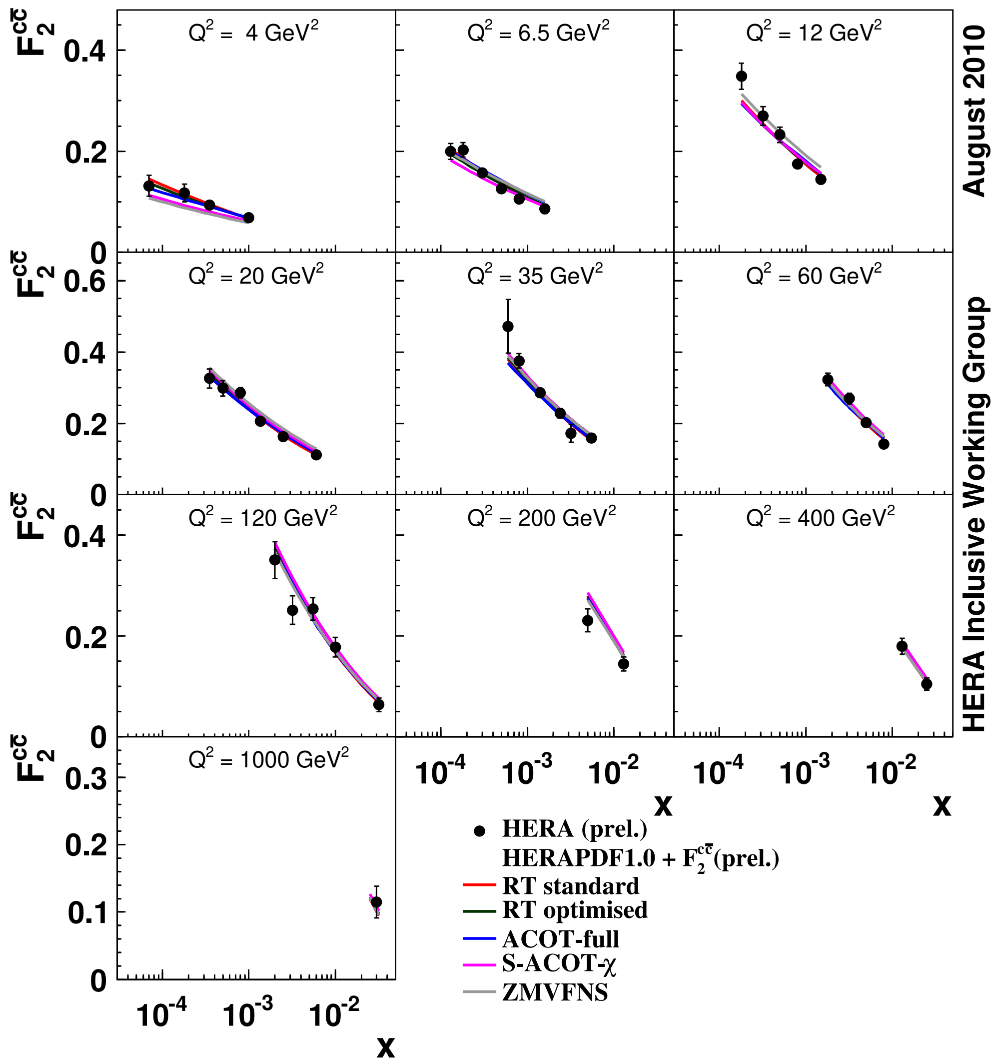

Figure 8: $F_2^{c\bar{c}}$ *as a function of x in* Q^2 *bins compared to QCD fits using different heavy flavour schemes obtained at* m_c^{model}(opt) *of each scheme. The data are shown with the uncorrelated uncertainties.*

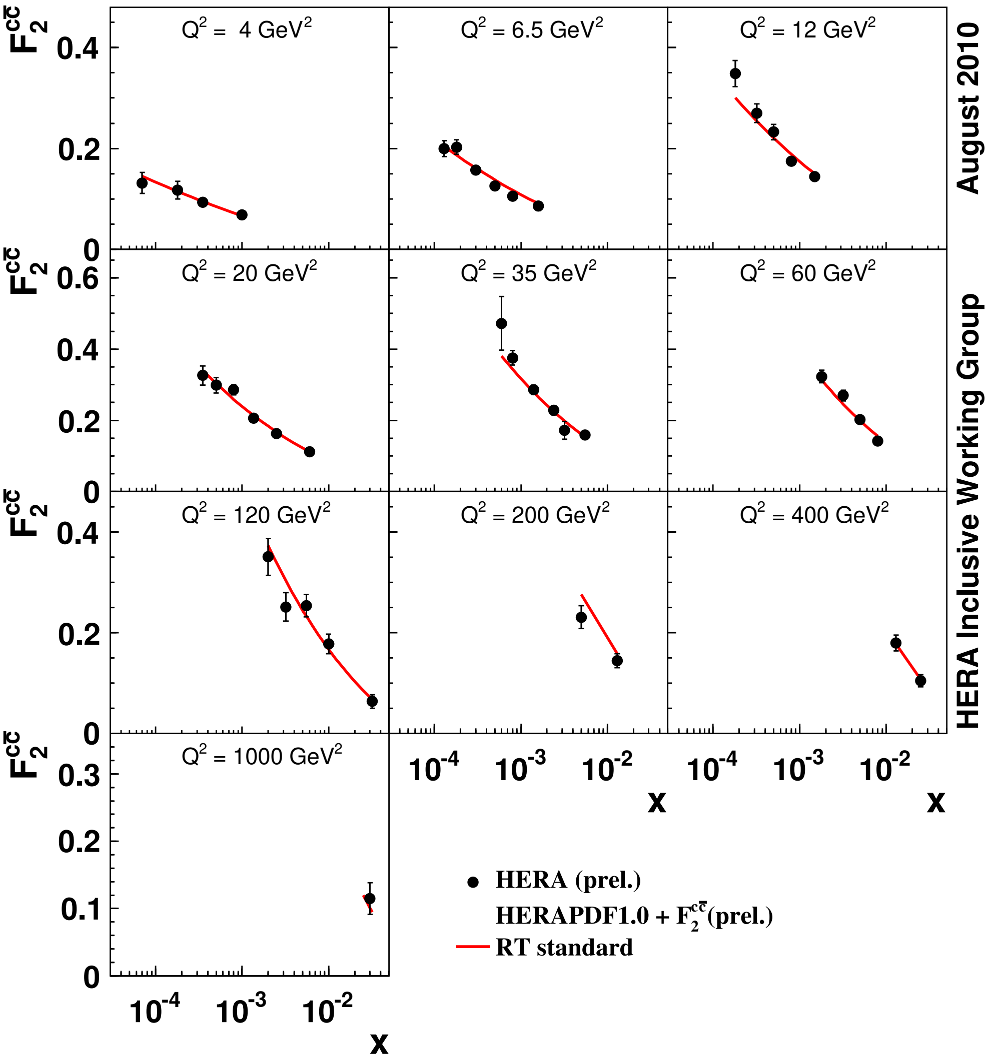

Figure 9: $F_2^{c\bar{c}}$ *as a function of x in* Q^2 *bins compared to QCD fit using the RT standard scheme obtained at* m_c^{model}(opt) . *The data are shown with the uncorrelated uncertainties.*

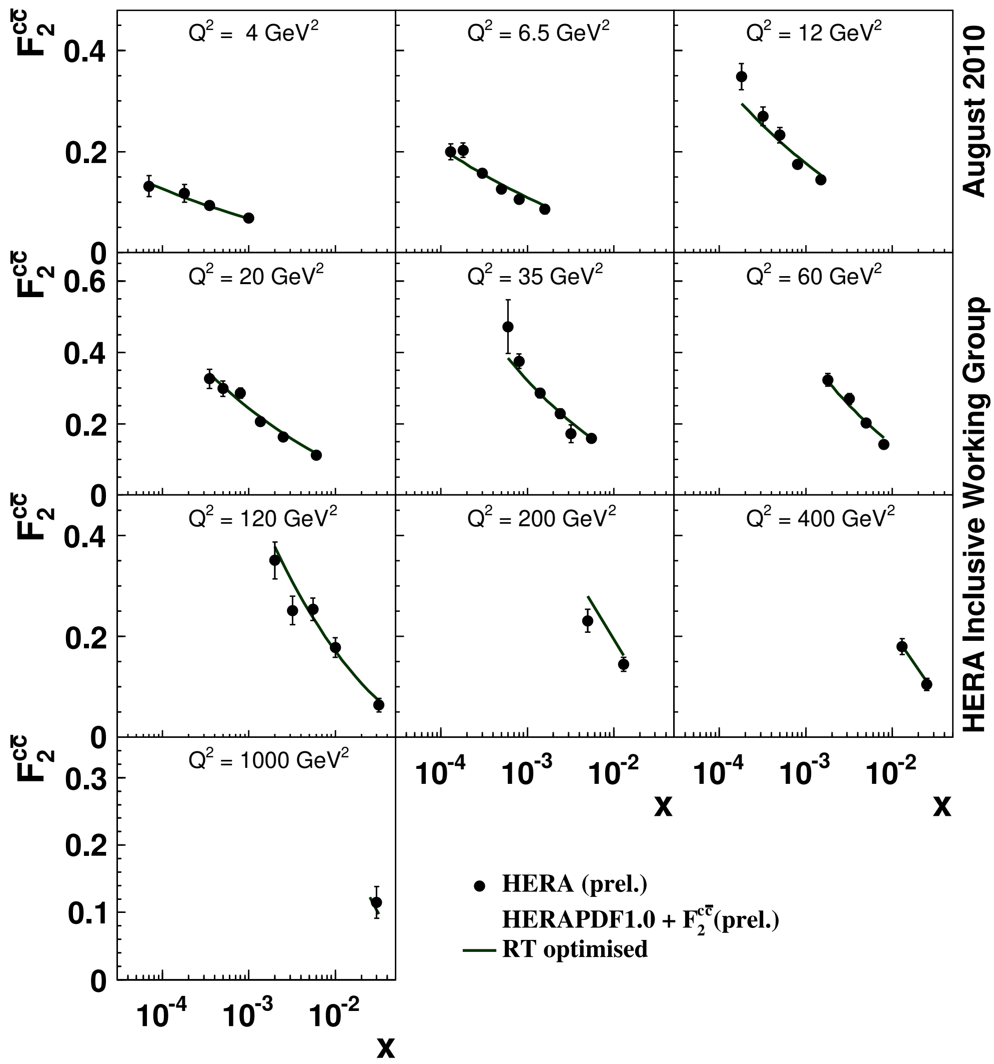

Figure 10: $F_2^{c\bar{c}}$ *as a function of x in* Q^2 *bins compared to QCD fit using the RT optimised scheme obtained at* m_c^{model}(opt) *. The data are shown with the uncorrelated uncertainties.*

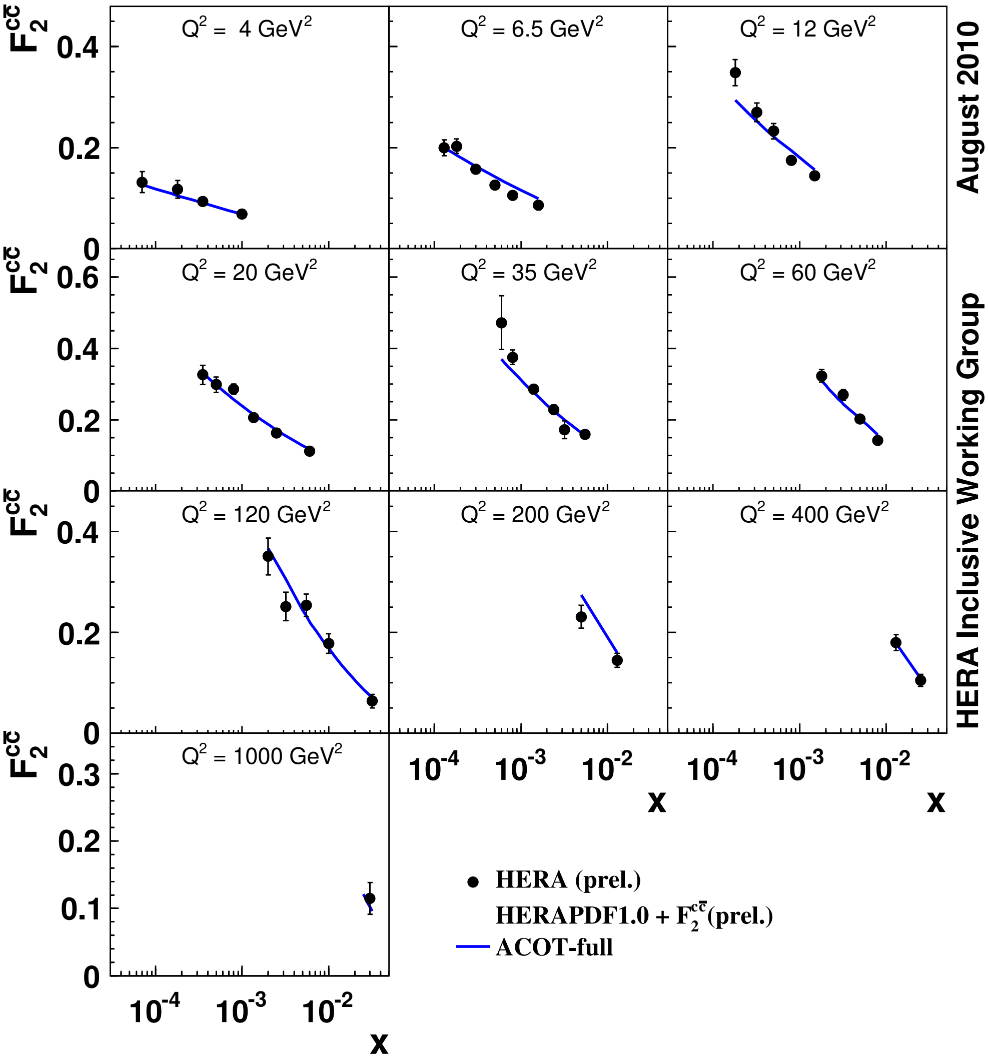

Figure 11: $F_2^{c\bar{c}}$ *as a function of x in* Q^2 *bins compared to QCD fit using the ACOT-full scheme obtained at* $m_c^{model}(\mathrm{opt})$ *. The data are shown with the uncorrelated uncertainties.*

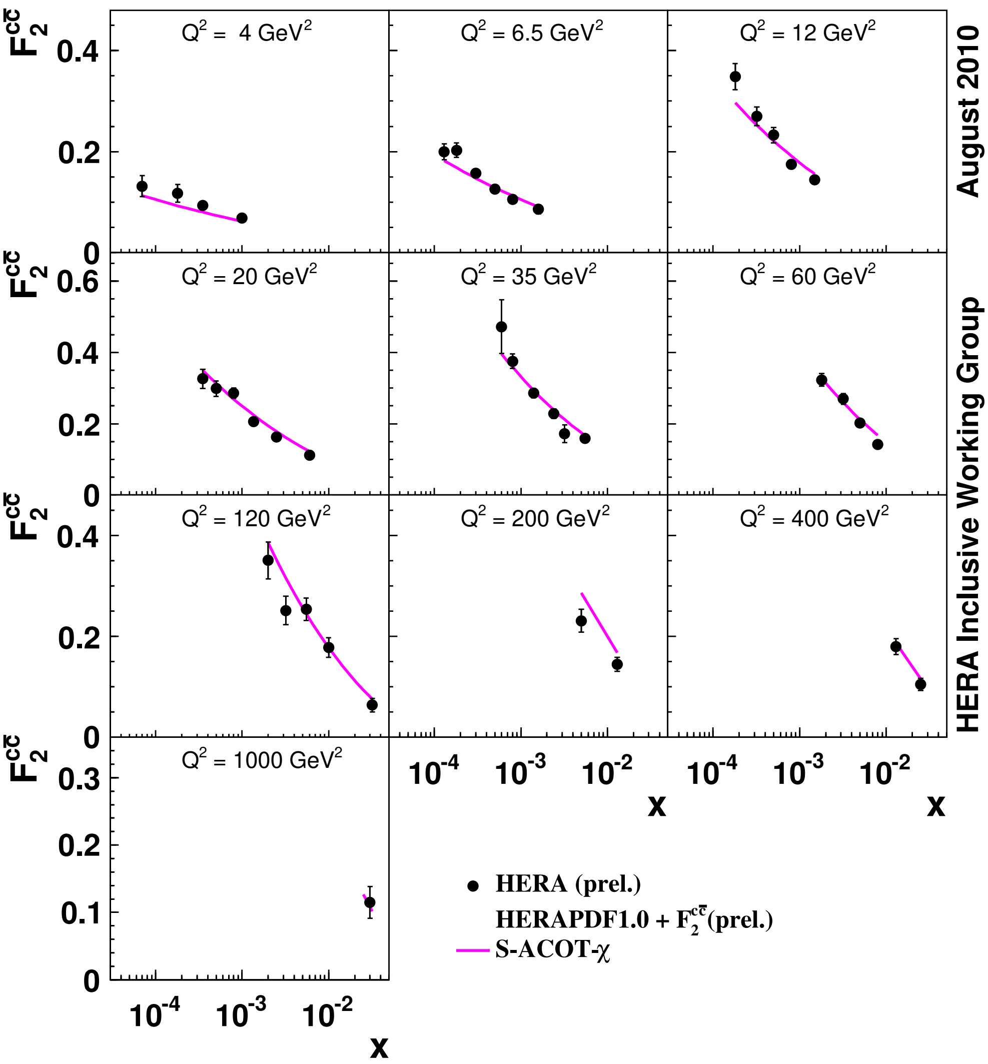

Figure 12: $F_2^{c\bar{c}}$ *as a function of x in* Q^2 *bins compared to QCD fit using the S-ACOT-*χ *scheme obtained at* $m_c^{model}(\text{opt})$. *The data are shown with the uncorrelated uncertainties.*

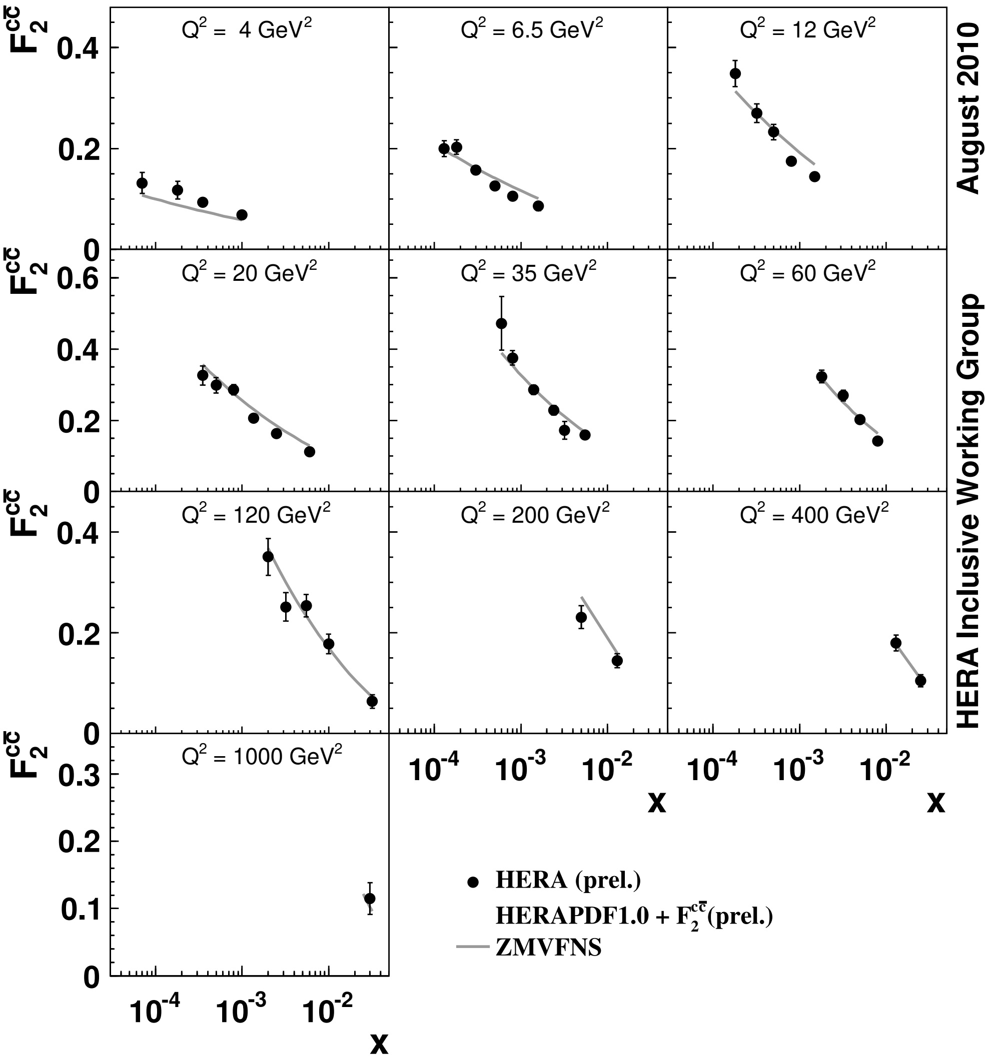

Figure 13: $F_2^{c\bar{c}}$ *as a function of x in* Q^2 *bins compared to QCD fit using the ZMVFN scheme obtained at* $m_c^{model}(\mathrm{opt})$ *. The data are shown with the uncorrelated uncertainties.*

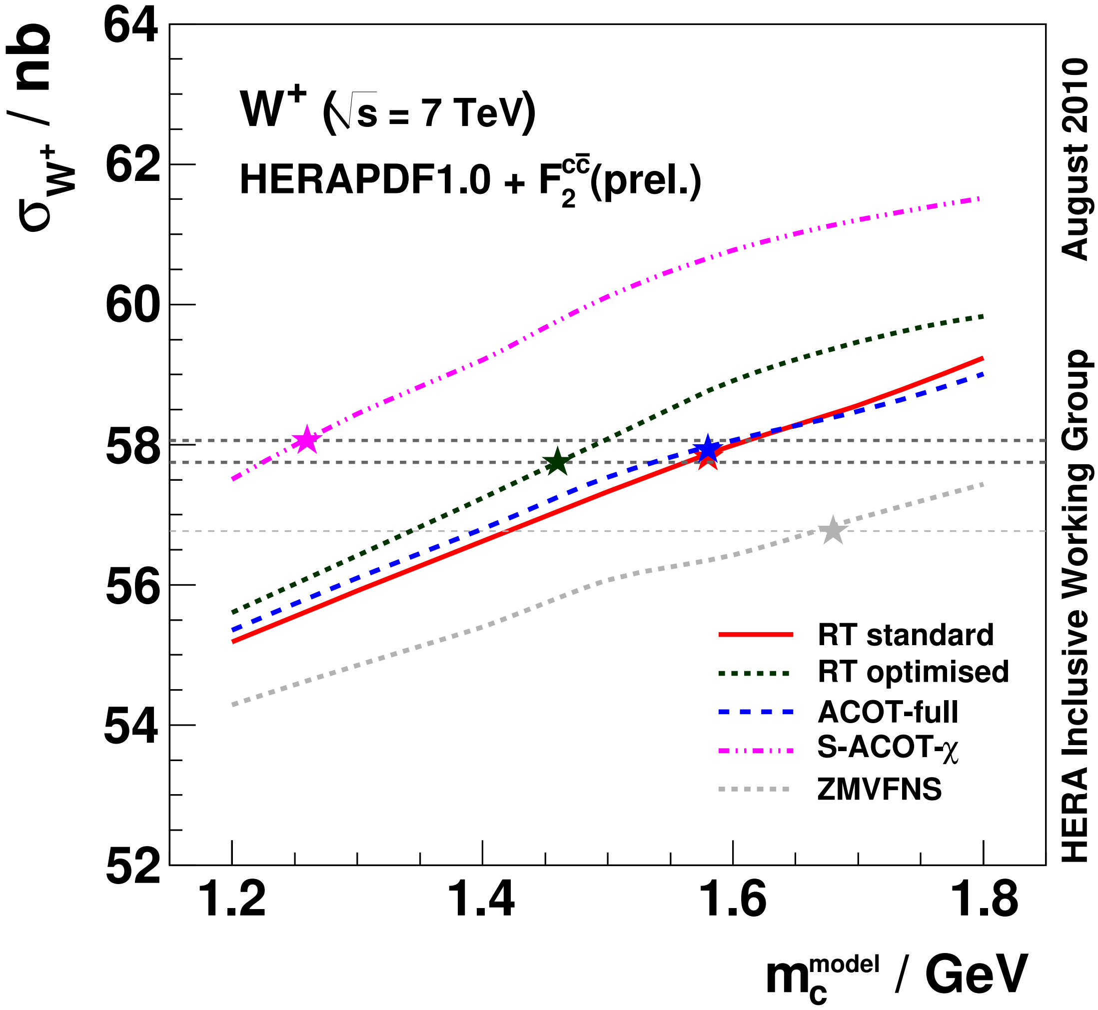

Figure 14: *W^+ production cross section σ_{W^+} at the LHC for $\sqrt{s}$ = 7 TeV as a function of m_c^{model}. The lines show predictions for different VFN schemes as inidcated by the legend. The stars show position of the corresponding m_c^{model}(opt) values. The thick dashed horizontal lines indicate the range of σ_{W^+}, determined for $m_c^{model} = m_c^{model}$(opt), if massive VFN schemes are considered. The thin dashed horizontal line corresponds to the prediction using ZMVFN scheme for $m_c^{model} = m_c^{model}$(opt).*

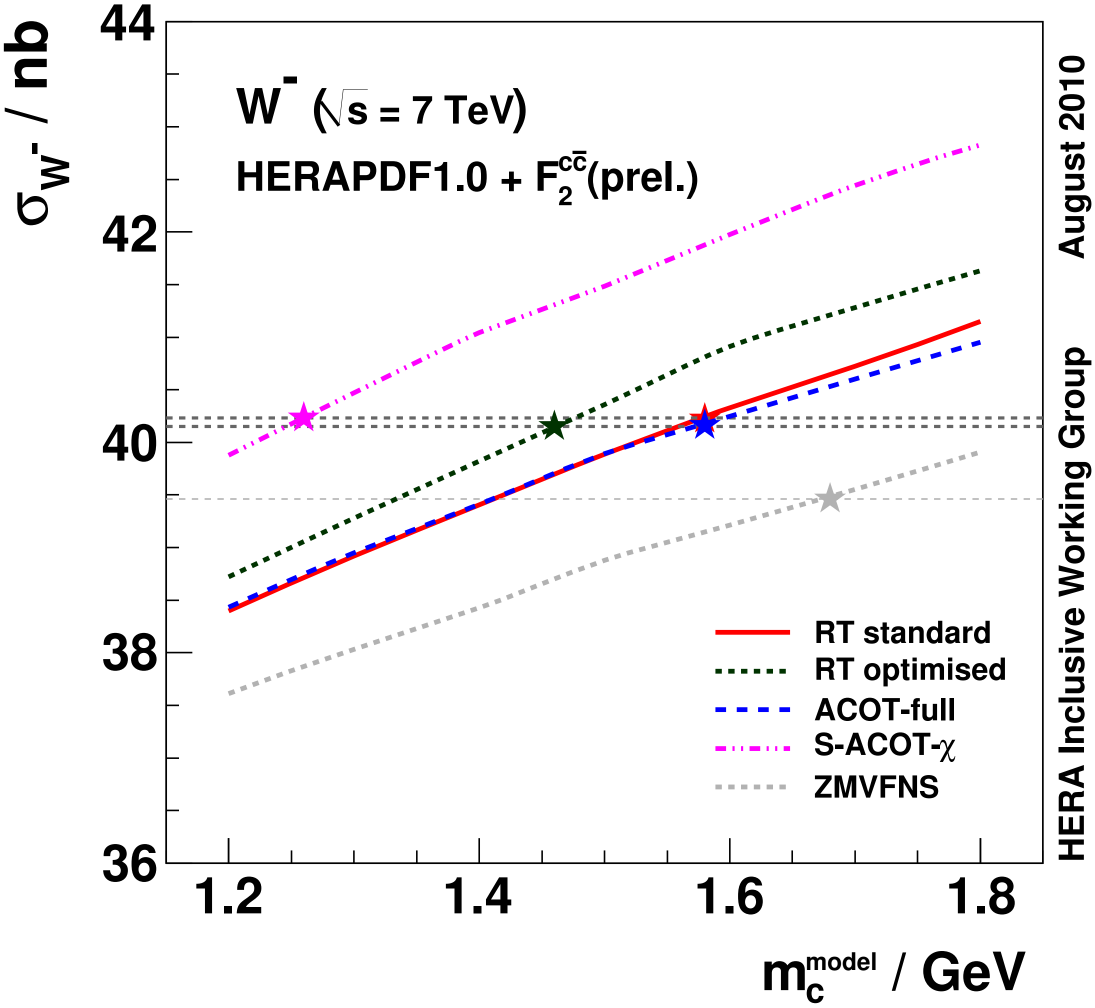

Figure 15: *W^- production cross section σ_{W^-} at the LHC for $\sqrt{s}$ = 7 TeV as a function of m_c^{model}. The lines show predictions for different VFN schemes as inidcated by the legend. The stars show position of the corresponding m_c^{model}(opt) values. The thick dashed horizontal lines indicate the range of σ_{W^-}, determined for $m_c^{model} = m_c^{model}$(opt), if massive VFN schemes are considered. The thin dashed horizontal line corresponds to the prediction using ZMVFN scheme for $m_c^{model} = m_c^{model}$(opt).*

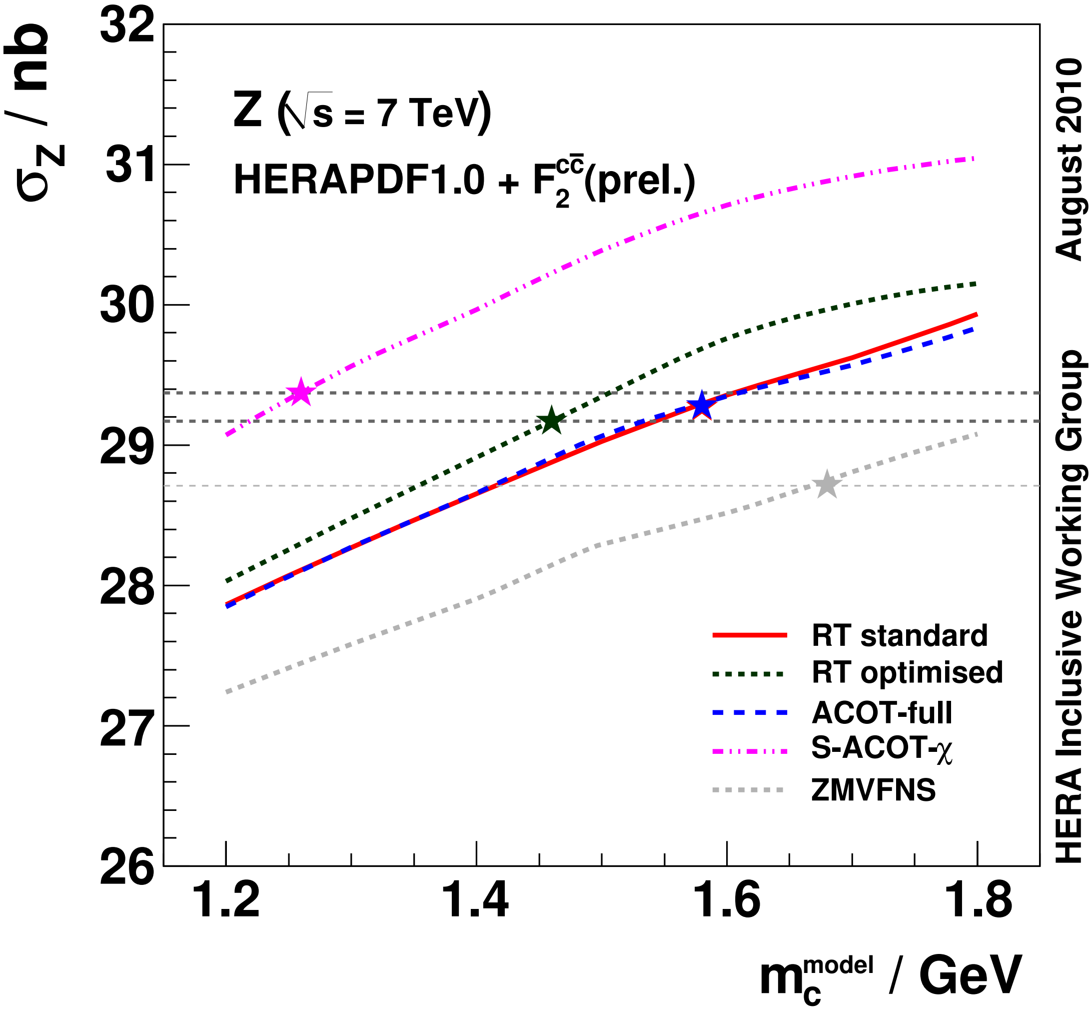

Figure 16: *Z production cross section σ_Z at the LHC for $\sqrt{s}$ = 7 TeV as a function of m_c^{model}. The lines show predictions for different VFN schemes as inidcated by the legend. The stars show position of the corresponding m_c^{model}(opt) values. The thick dashed horizontal lines indicate the range of σ_Z, determined for $m_c^{model} = m_c^{model}$(opt), if massive VFN schemes are considered. The thin dashed horizontal line corresponds to the prediction using ZMVFN scheme for $m_c^{model} = m_c^{model}$(opt).*